Structural Studies, Thermochromic Luminescent Properties and Crystal-to-Crystal Transformation of a Double-stranded Cu^{I}-I-Bisquinoline Coordination Polymer

Cristian Pinzón-Vanegas,[a] Jorge J. Villa-Rivera,[a] Víctor Sánchez-Mendieta,[b] Diego Martínez-Otero,[b] Joaquín Barroso-Flores,[b] Alfredo R. Vilchis-Nestor,[b] Ginés Lifante-Pedrola,[c] Pilar Amo-Ochoa[d,e] and Alejandro Dorazco-González[a*]

[a] *Institute of Chemistry, National Autonomous University of Mexico, Mexico City 04510.*
[b] *Centro Conjunto de Investigación en Química Sustentable, UAEM-UNAM, Carretera Toluca-Atlacomulco Km 14.5, C. P. 50200, Toluca, Estado de México, México, Instituto de Química, Universidad Nacional Autónoma de México.*
[c] *Dpto. Física Aplicada, Universidad Autónoma de Madrid, 28049 Madrid, Spain.*
[d] *Dpto. de Química Inorgánica. Universidad Autónoma de Madrid, 28049, Madrid, Spain.*
[e] *Institute for Advanced Research in Chemical Sciences (IAdChem). Universidad Autónoma de Madrid, 28049, Madrid, Spain.*

ELECTRONIC SUPPORTING INFORMATION

Table S1. Crystallographic data collection for **CP1**$_{100K}$, **CP1**$_{150K}$, **CP1**$_{293K}$ and **CP2**
Table S2. Selected bond lengths and angles for **CP1** at 100 K and at 293 K
Table S3. H-bonds for **CP1** [Å and °] inside the X-crystal structure at 100 K
Table S4. Elemental analysis of **CP1** and **CP1**-G
Table S5. Selected bond lengths and angles for **CP2**
Table S6. H-bonds for **CP2** [Å and °] inside the X-crystal structure
Table S7. Selected excited states calculated at the TD-DFT M05-2X/LANL2DZ //cc-pVTZ (Iodine) level of theory for **CP1** and **CP2**.
Fig. S1. ^{1}H-NMR spectrum of L in DMSO-d_6.
Fig. S2 ^{13}C-NMR spectrum of L in DMSO-d_6.
Fig. S3. IR-ATR spectrum and MS (DART+) of L.
Fig. S4. Cluster like-staircase of Cu^{I}-I in **CP1** along *c* axis
Fig. S5. H-bonds and π-π stacking interactions in crystal structure of **CP1**.
Fig. S6. Interaction of CH_3CN with **CP1** inside the voids.
Fig. S7. CP1 growing along the *b* axis and the formation of CH_3CN channels.
Fig. S8. IR-ATR spectra of L and **CP1**.
Fig. S9. SEM images of the single crystals of **CP1**.
Fig. S10. TGA curve of crystalline sample of **CP1**.
Fig. S11. Solid state UV-vis absorption spectrum of **CP1**.
Fig. S12. Emission (λ_{ex}= 413 nm) spectra of solid-state sample of **CP1** at 100 K and 298 K.
Fig. S13. IR-ATR of crystalline unground sample (**CP1**), ground samples (**CP1**-G) and treated samples with CH_3CN vapors (**CP1**-R) for 3 cycles
Fig. S14. SEM micrographs of unground sample **CP1**, ground samples (**CP1**-G) and treated samples with CH_3CN (**CP1**-R) for 3 cycles.
Fig. S15. Emission spectra of **CP1**-G at room temperature and **CP1** at 100 K.
Fig. S16. PXRD (Cu K_α) patterns of the SCSC transformation from **CP1** to **CP2**.
Fig. S17. PXRD (Cu K_α) patterns of **CP1**, **CP2** and **CP1** at ~ 40 °C.
Fig. S18. IR-ATR spectra of starting **CP1** and **CP1** regenerated from **CP2** in CH_3CN.
Fig. S19. DFT optimized structure of **CP1**.
Fig. S20. Molecular orbitals (MOs) of **CP1** at 100 K.
Fig. S21. UV-vis plot of **CP1** calculated with the TD-DFT method.
Fig. S22. DFT optimized structure of **CP1** at 293 K.
Fig. S23. Molecular orbitals (MOs) of **CP1** at 293 K.
Fig. S24. UV-vis plot of **CP2** calculated with the TD-DFT method.

Materials, reagents and equipment

***Chemical synthesis of L*:** The synthetic methodology previously reported[1,2] was modified as follows. In a flask of 100 mL, 125.36 mg (0.59 mmol) of 2,6-pyridinedicarbonyl dichloride were dissolved in 10 mL of dry CH_3CN. Then, 144.17 mg (1.25 mmol) of 3-aminoquinoline in 10 mL of dry CH_3CN was slowly added to the previous solution. The reaction was left under reflux and stirring for 6 h. After the reaction, the bright-yellow solid was dried and neutralized with 50 mL of one aqueous solution of $NaHCO_3$ (3% w-v) and the color changed to pale-yellow. The product was filtrated and washed twice with 10 mL of bi-distilled water and once with 10 mL of CH_3CN. Yield 82.72%. ^{1}H NMR (300 MHz, 25 °C, DMSO-d_6) δ (ppm) 11.47 (s, 2H), 8.97 (dd, *J*= 4.2, 1.5 Hz, 2H), 8.55 – 8.33 (m, 5H), 8.02 (d, *J*= 8.2 Hz, 2H), 7.84 (dt, *J*= 14.5, 7.4 Hz, 4H), 7.64 (dd, *J*= 8.6, 4.2 Hz, 2H). ^{13}C NMR (300 MHz, 25 °C, DMSO-d_6) δ (ppm) 162.71, 150.79, 148.49, 148.11,140.16, 133.27, 132.21, 129.06, 127.67, 125.44, 124.49, 124.42, 121.40. ESI (+)-MS (m/z): calculated for $[C_{25}H_{18}N_5O_2]^+$: 420, found: 420. ATR-IR ν (cm^{-1}): 3474.70 (w, ν); 3347.62-2976.92 (w, ν); 1676.23 (s, ν); 1533.77 (s, ν); 1492.49 (s, δ).

Reagents and solvents: CuI (Aldrich, ≥ 99.5%) and CH_3CN (Scharlau, UV HPLC grade).

***Equipment and software**:* Powder X-Ray Diffraction (PXRD) data were collected using a PANalytical X'Pert PRO diffractometer equipped with a θ/2θ primary monochromator and X'Celerator fast detector and 1° for Kα1 monochromator. The samples were analyzed with scanning θ/2θ, from 3–50 degrees, with an angular increase of 0.0167 and a time per increment of 100 s. A Hitachi S-3000N. Fourier Transform Infrared (IR-ATR) absorption spectra were recorded in the range of 4000–600 cm^{-1} by using the standard Pike ATR cell on a Bruker Tensor 27 FT-IR spectrophotometer (Bruker Optik GmbH, Ettlingen, Germany). Micrography and composition of the polymers were obtained using a JSM-610LV microscope from JEOL (JEOL, Ltd, Akishima, Tokyo, Japan) operated at 20 kV and equipped with a Bruker QUANTAX 200 Energy-Dispersive X-ray Spectrometer (EDS) (Bruker Nano GmbH, Adlershof. Berlin, Germany) for elemental characterization for **CP1**, and a Hitachi S-3000N SEM-EDX microscope for **CP1** microcrystals and **CP1**-G. The chemical compositional of the polymers was obtained by elemental analyses with a Thermo Scientific/Flash 2000 elemental analyzer. The thermogravimetric analysis (TGA) measurements were realized in Instruments Q500 with thermobalance oven with a platinum sample holder. The experiment was carried out under a N_2 atmosphere at a flow rate of 90 mL min^{-1} and a heating rate of 10 °C min^{-1}, in a temperature range of 25 to 1000 °C. Luminescence spectra at room temperature were recorded on a photoluminescence spectrometer FLS 1000 from Edinburgh Instruments. Excitation and emission spectra were recorded in solid samples to different temperatures from nitrogen liquid temperature (80 K) to room temperature (293 K) with a cryostat equipped with a vacuum pump to the polycrystalline powders, in the spectral range of 300−1000 nm using a Spex Fluorolog II equipped with a 450 W Xe lamp as the excitation source, two 0.22 m monochromators (Spex 1680) for wavelength selection of the excitation and emission light, respectively.

Absolute quantum yield measurements (Φ) were performed on an FLS920 from Edinburgh Instruments equipped with a $BaSO_4$-coated integrating sphere, a Xenon lamp (450W Xe900) and a detector R928P PMT.

Lifetime Measurements. A custom-built Fluorescence Lifetime Imaging Microscope system was used to acquire the fluorescence lifetimes. A 405 nm laser pulsed at 10 MHz (LDH-PFA- 355, PicoQuant) was focused with a 0.40 NA reflective objective (LMM-40X-UVV-160, ThorLabs) into a 1.0 cm quartz cell or directly on

the crystalline sample in case of measurements in solid-state. The epifluorescence passed through a 425 nm long-pass dichroic mirror (Chroma T425lpxr-UF2), a 405 nm notch filter (Chroma ZET405nf), a 425 nm long pass emission filter (Chroma ET425lp) and was focused to single photon avalanche photodiode (PD-050-CTE, MPD). The laser controller (PDL-800-D, PicoQuant) and the detector were connected to a TCSPC card (PicoHarp 300, PicoQuant). The intensity of irradiation was set to obtain less than 1% of detection events. Back-scattered light
from a mirror was used to obtain the IRF under the same conditions of irradiation. All data were obtained and treated in SymphoTime 64 software (PicoQuant).

***Computational Details**:* All calculations were carried out with the Gaussian 16 suite of programs[3] at the M052X/LANL2DZ // cc-pVTZ (for Iodine) level of theory with the corresponding pseudopotentials for Cu and I. UV-Vis spectra were calculated using the Time Dependent (TD-DFT) version of the aforementioned methods (80 excited states were requested to properly describe low energy excitations); all plots were made therefrom with the in-house UVEH-Vis code.[4] Starting from their crystallographic coordinates, positions for hydrogen atoms were optimized previous to population analysis and excited states calculations.

cc-pVDZ-PP basis set and pseudopotential for iodine.
Basis Set Exchange, Version 0.11
https://www.basissetexchange.org
Basis set: cc-pVDZ-PP
Description: cc-pVDZ-PP
Role: orbital
Version: 0 (Data from the original Basis Set Exchange)

```
I    0
S    8   1.00
     2.449790D+03          4.190000D-04
     3.598080D+02          2.240000D-03
     1.440580D+01          3.972230D-01
     9.076320D+00         -9.322490D-01
     2.088100D+00          9.371380D-01
     1.034980D+00          3.920860D-01
     3.162840D-01          1.248500D-02
     1.217190D-01         -1.329000D-03
S    1   1.00
     3.162840D-01          1.000000D+00
S    8   1.00
     2.449790D+03          1.750000D-04
     3.598080D+02          1.057000D-03
     1.440580D+01          1.690000D-01
     9.076320D+00         -4.217930D-01
     2.088100D+00          6.388640D-01
     1.034980D+00          3.201150D-01
     3.162840D-01         -8.144280D-01
     1.217190D-01         -4.897980D-01
S    1   1.00
     1.217190D-01          1.000000D+00
P    6   1.00
     1.953010D+01          5.893400D-02
     1.108820D+01         -2.309300D-01
     2.715630D+00          6.648010D-01
     1.204300D+00          4.506730D-01
```

```
     3.399450D-01          2.898000D-02
     1.108810D-01         -2.889000D-03
P    6   1.00
     1.953010D+01         -1.883600D-02
     1.108820D+01          8.000600D-02
     2.715630D+00         -3.066520D-01
     1.204300D+00         -1.475940D-01
     3.399450D-01          6.075060D-01
     1.108810D-01          5.470490D-01
P    1   1.00
     1.108810D-01          1.000000D+00
D    6   1.00
     4.547650D+01          4.266000D-03
     1.319280D+01         -1.362500D-02
     4.227410D+00          3.097560D-01
     1.942800D+00          5.097720D-01
     8.397710D-01          2.974610D-01
     3.000000D-01          4.016400D-02
D    1   1.00
     3.000000D-01          1.000000D+00
****
I    0
I-ECP    4    28
g potential
1
2      1.00000000           0.00000000
s-g potential
3
2     40.03337600          49.98964900
2     17.30057600         281.00655600
2      8.85172000          61.41673900
p-g potential
4
2     15.72014100          67.41623900
2     15.20822200         134.80769600
2      8.29418600          14.56654800
2      7.75394900          28.96842200
d-g potential
4
2     13.81775100          35.53875600
2     13.58780500          53.33975900
2      6.94763000           9.71646600
2      6.96009900          14.97750000
f-g potential
4
2     18.52295000         -20.17661800
2     18.25103500         -26.08807700
2      7.55790100          -0.22043400
2      7.59740400          -0.22164600
```

Table S1. Crystallographic data collection for **CP1$_{100K}$**, **CP1$_{150K}$**, **CP1$_{293K}$** and **CP2**.

	CP1$_{100K}$	**CP1$_{150K}$**	**CP1$_{293K}$**	**CP2**
Formula	$C_{27}H_{20}CuIN_6O_2$	$C_{27}H_{23}CuIN_7O_2$	$C_{27}H_{20}CuIN_6O_2$	$C_{25}H_{17}CuIN_5O_2$
Formula weight	646.58	667.96	650.93	609.88
T (K)	100(2)	150(2)	293(10)	275(10)
Crystal system	Monoclinic	Monoclinic	Monoclinic	Monoclinic
Space group	C2/c	C2/c	C2/c	$P2_1/c$
a (Å)	54.117(2)	54.126(4)	54.3406(7)	24.5179(2)
b (Å)	11.8772(5)	11.9193(9)	11.9630(2)	12.1034(10)
c (Å)	7.4089(3)	7.4457(5)	7.55950(10)	7.5341(10)
α (°)	90	90	90	90
β (°)	96.1828(8)	96.286(2)	96.7230(10)	95.3220(10)
γ (°)	90	90	90	90
Volume (Å^3)	4734.4(3)	4774.7(6)	4880.46(12)	2226.11(4)
Z	8	8	8	4
d_{calc} (g cm^{-3})	1.814	1.858	1.772	1.820
μ (mm^{-1})	2.359	2.251	11.516	12.560
F (000)	2545	2656	2576	1200
Total reflections	31823	7721	45832	41076
Unique reflections	5443	7721	5231	4072
Observed data [I > 2σ (I)]	5443	7721	4547	9785
N° of parameters	426	381	308	307
R_{int}	0.0304	0.0554	0.0581	0.0299
R_1, wR_2 [I > 2σ (I)]	0.0317, 0.0839	0.0670, 0.1504	0.0708, 0.2000	0.0350, 0.0918
R_1, wR_2 (all data)	0.0341, 0.0857	0.0772, 0.1556	0.0764, 0.2040	0.0371, 0.0932

Table S2. Selected bond lengths and angles for **CP1** at 100 K and at 293 K.

	$CP1_{100K}$	**$CP1_{150K}$**	**$CP1_{293K}$**
Bond	Lengths (Å)		Lengths (Å)
I(1)-Cu(1)	2.5870(4)	2.5812(12)	2.5823(14)
I(1)-Cu(1)#2	2.9025(5)	2.8988(14)	2.9079(19)
I(2)-Cu(1)	2.6424(5)	2.6478(14)	2.6515(16)
Cu(1)-N(3)	2.037(2)	2.034(6)	2.042(16)
Cu(1)-Cu(1)#1	2.8482(8)	2.885(2)	2.970(3)
Bond	Angles (°)		Angles (°)
N(3)-Cu(1)-I(1)	127.59(7)	128.19(18)	128.64(18)
N(3)-Cu(1)-I(2)	109.10(7)	108.70(19)	108.68(19)
N(3)-Cu(1)-I(1)#3	95.47(7)	95.71(19)	96.34(19)
I(1)-Cu(1)-I(2)	113.987(15)	113.01(4)	110.82(6)
I(1)-Cu(1)-I(1)#3	104.081(14)	105.05(4)	106.83(6)
I(2)-Cu(1)-I(1)#3	100.857(13)	100.79(4)	100.95(5)
Cu(1)-I(1)-Cu(1)	66.800(18)	67.95(5)	70.22(7)
Cu(1)-I(2)-Cu(1)	65.222(17)	66.02(5)	68.13(6)

Table S3. H-bonds for **CP1** [Å and °] inside the X-crystal structure.

D-H···A	**d(D-H)**	**d(H...A)**	**d(D...A)**	**<(DHA)**
N(8)-H(8)···O(1)#1	0.80(4)	2.28(4)	2.940(4)	140(4)
N(8)-H(8)···N(1)	0.80(4)	2.36(4)	2.744(4)	111(4)
N(10)-H(10)···N(1)	0.78(4)	2.25(4)	2.695(4)	117(4)
C(13)-H(13)···Br(1)#2	0.95	3.03	3.833(4)	143.7
C(16)-H(16)···O(1)	0.95	2.35	2.867(4)	113.7
C(23)-H(23)···Br(1)#3	0.95	3.12	3.831(3)	133.4
C(26)-H(26)···O(2)	0.95	2.30	2.889(4)	119.4

Symmetry transformations used to generate equivalent atoms: #1 x,-y+1/2,z-1/2 #2 -x+1,y+1/2,-z+1/2 #3 -x+1,-y+1,-z

Table S4. Elemental analysis of **CP1** and **CP1**-G

	Elemental analysis		
	%C	%H	%N
CP1	49.04	2.85	11.43
CP1-G	48.15	2.89	11.11

Table S5. Selected bond lengths and angles for **CP2**

Lengths		**Angles**	
Bond	(Å)	Bond	(°)
Cu(1)-I(1)	2.5044(7)	I(1)-Cu(1)-I(1)#2	108.90(2)
Cu(1)-I(1)#2	2.5320(7)	N(3)-Cu(1)-I(1)#2	123.71(9)
Cu(1)-N(3)	1.978(3)	N(3)-Cu(1)-I(1)	127.38(9)

Table S6. H-bonds for **CP2** [Å and °]

D-H···A	**d(D-H)**	**d(H...A)**	**d(D...A)**	**<(DHA)**
C(8)-H(8)···O(1)	0.93(4)	2.38(4)	2.864(5)	112.3(4)
C(18)-H(18)···O(2)	0.93(4)	2.32(4)	2.897(5)	119.4(4)
N(2)-H(2A)···O(1)	0.86(4)	2.35(4)	2.962(4)	128.9(4)
N(4)-H(4A)···N(1)	0.86(4)	2.26(4)	2.688(4)	110.7(4)

Symmetry transformations used to generate equivalent atoms: #1 x, 1/2-y, 2+z

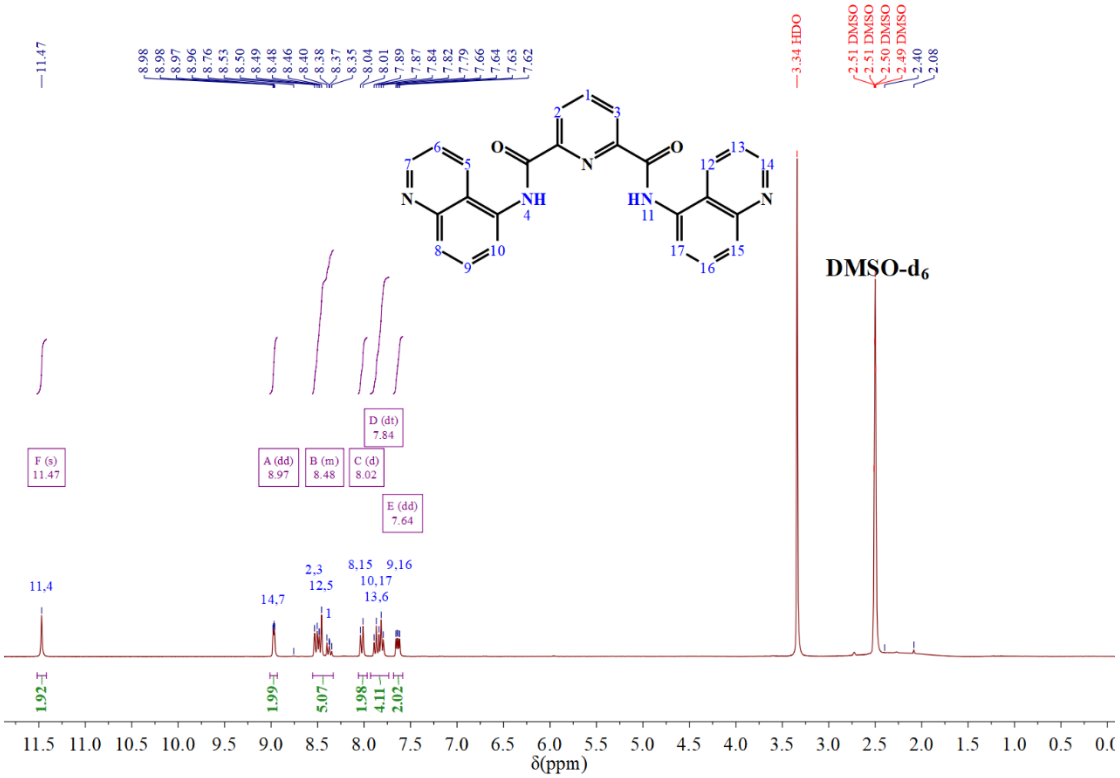

Fig. S1. [1]H-NMR spectrum (298 K, 25 °C, 300 MHz) of **L** in DMSO-d_6.

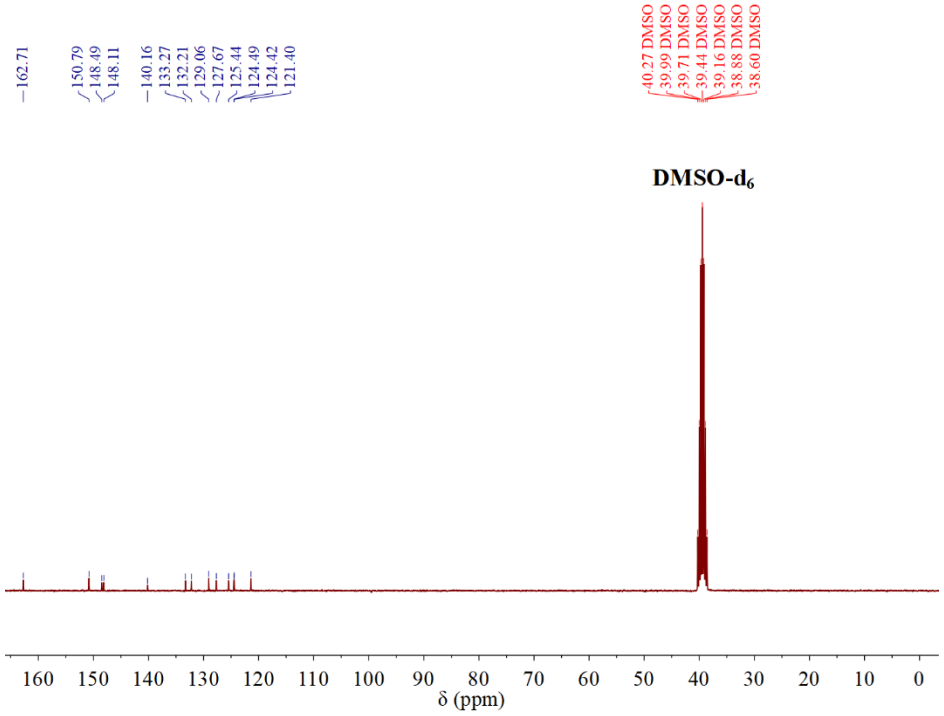

Fig. S2 [13]C-NMR spectrum (298 K, 25 °C, 300 MHz) of **L** in DMSO-d_6.

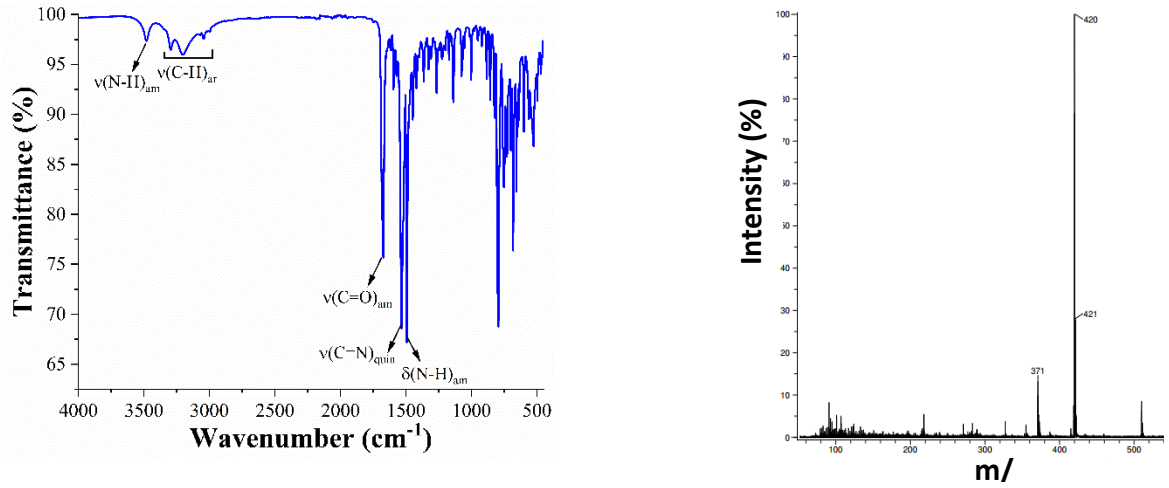

A B

Fig. S3. A) IR-ATR spectrum and B) Positive scan MS-(DART+) spectrum of L.

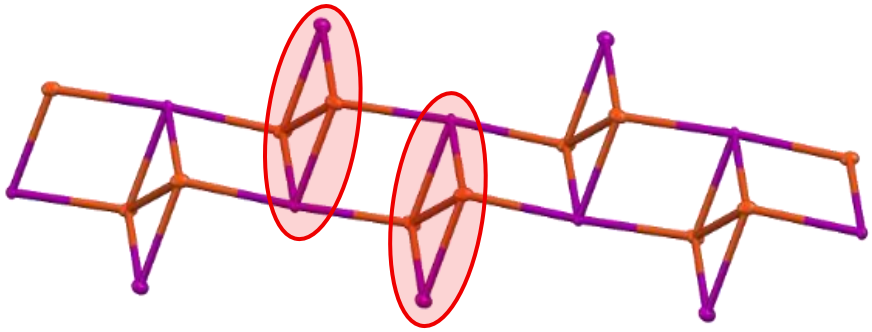

Fig. S4. Cluster like-staircase of Cu^{I}-I along *c* axis in **CP1** (hydrogen are omitted for clarity and ellipsoids are at 30% of probability).

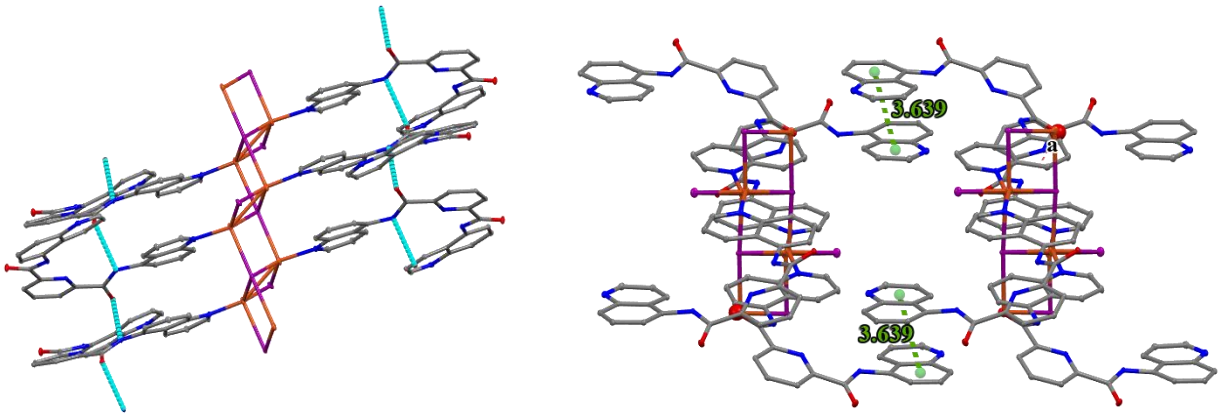

A B

Fig. S5. A) Hydrogen bonding interactions (blue dashed lines) in **CP1** along the *c* axis. B) π-π stacking interactions (green dashed lines) in **CP1** along the *a* axis showing centroid-centroid distances.

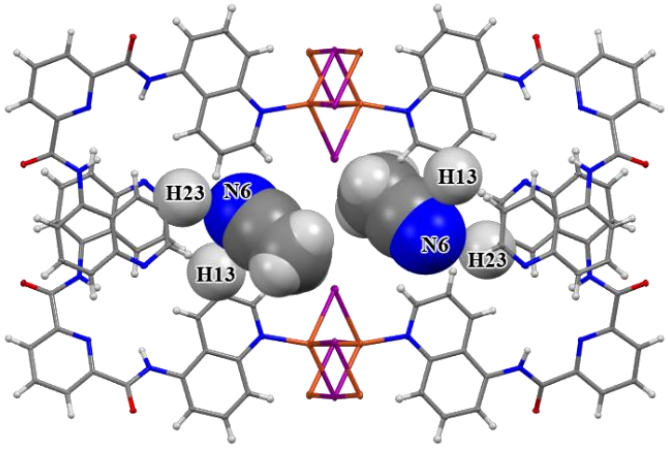

Fig. S6. Interaction of CH_3CN with **CP1** inside the voids.

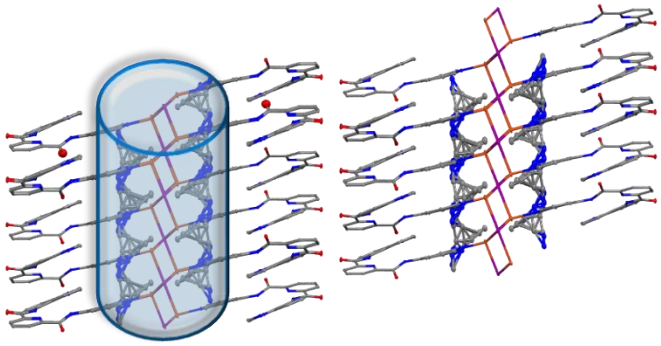

Fig. S7. CP1 growing along the *b* axis and the formation of CH_3CN channels.

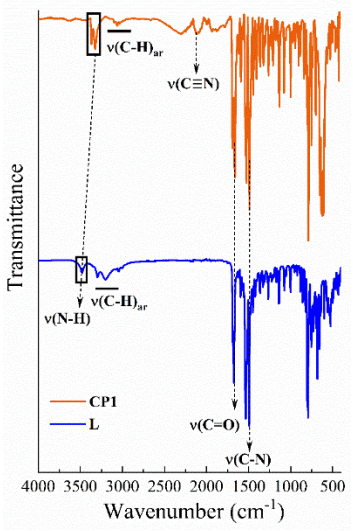

Fig. S8. IR-ATR (cm^{-1}) spectra of **L** (bottom) and **CP1** (top).

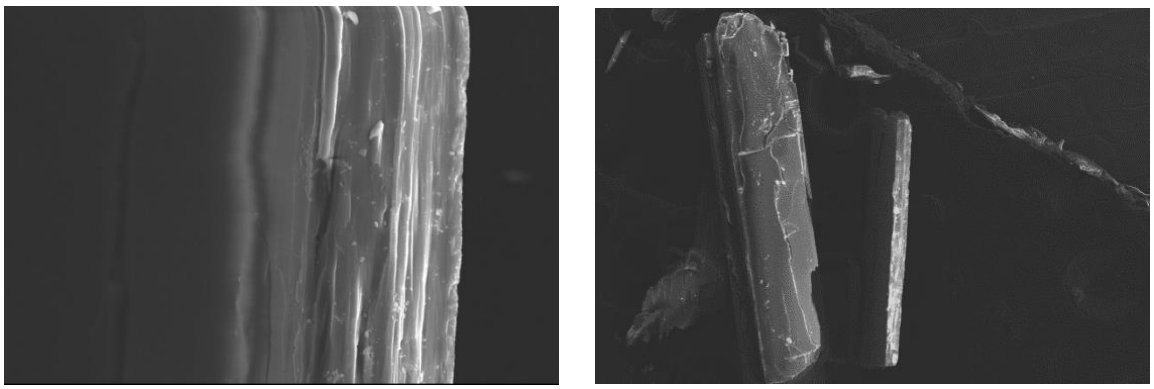

Fig. S9. SEM images of the single crystals of **CP1**.

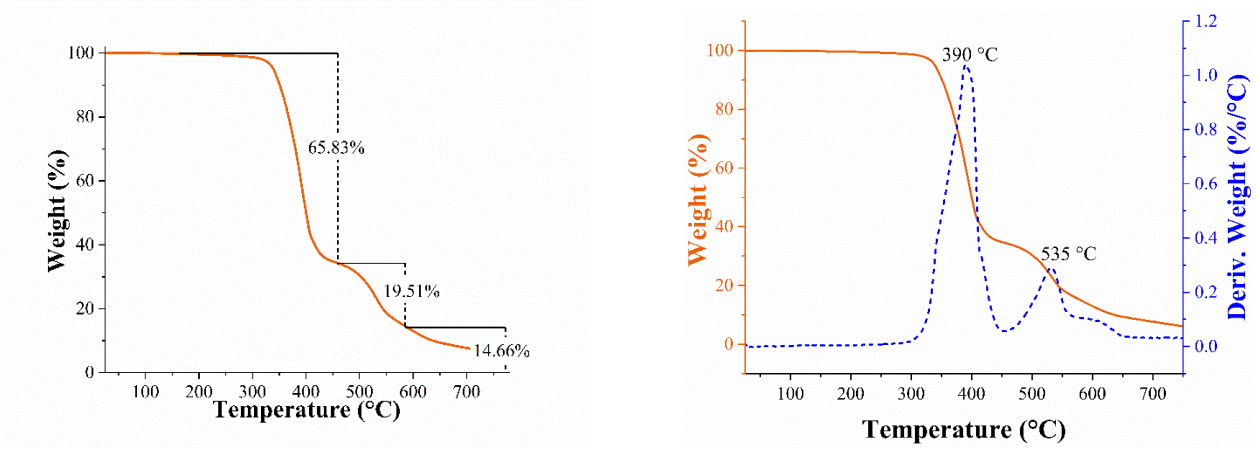

A B

Fig. S10. A) TGA curve of crystalline sample of **CP1**. B) thermogram and its derivative weight curve of **CP1.**

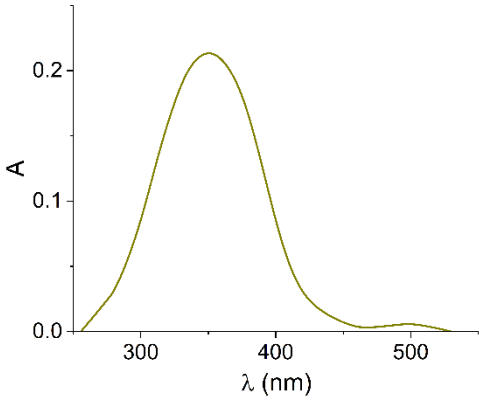

Fig. S11. Solid state UV-vis absorption spectrum of **CP1**.

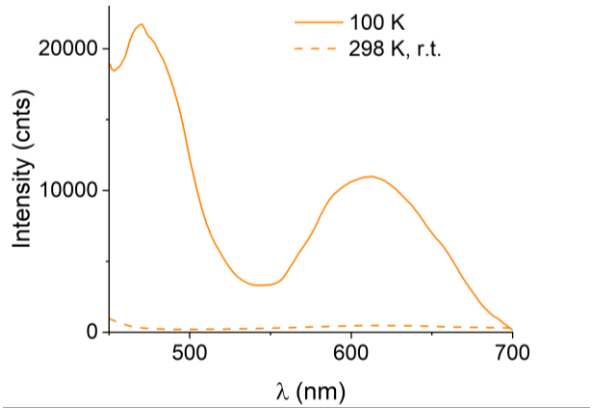

Fig. S12. Emission (λ_{ex}= 413 nm) spectra of solid-state sample of **CP1** at 100 K and 298 K.

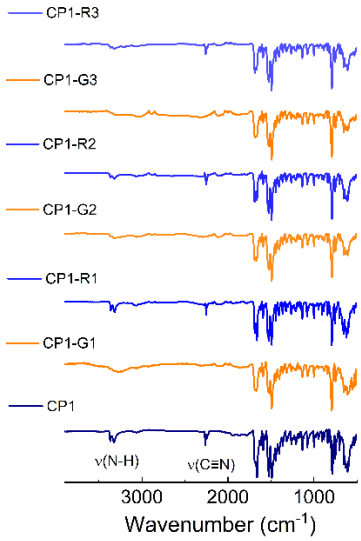

Fig. S13. IR-ATR of crystalline unground sample (**CP1**), ground samples (CP1-G) and treated samples with CH_3CN vapors (**CP1**-R) for 3 cycles.

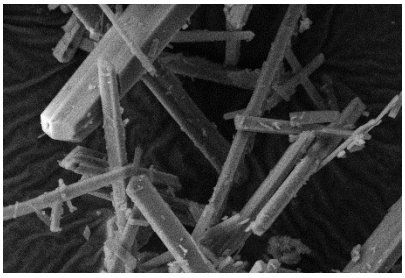

crystalline unground **CP1**

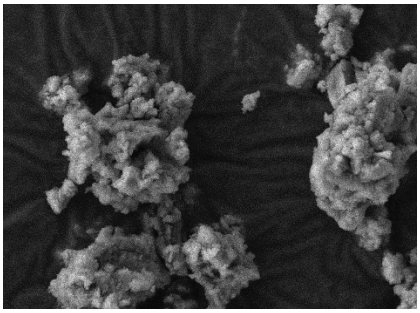

CP1-G1

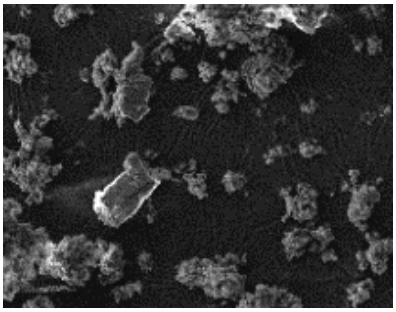

CP1-R

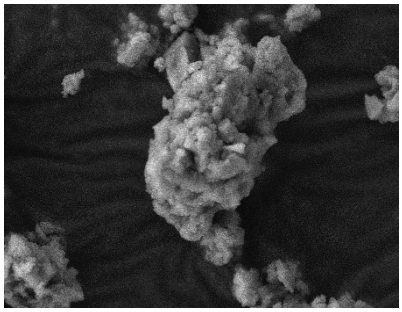

CP1-G2

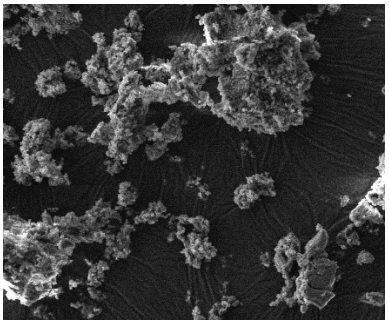

CP1-R2

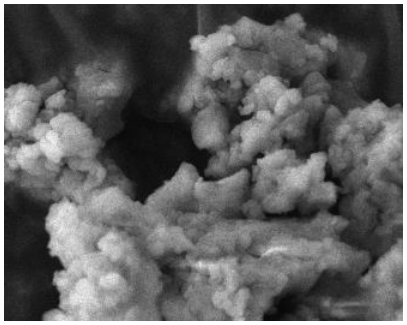

CP1-G3

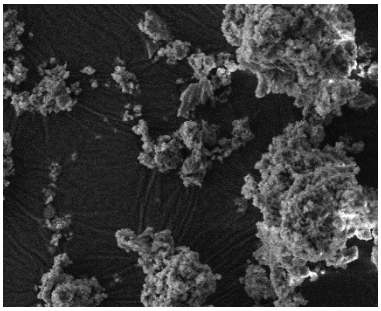

CP1-R3

Fig. S14. SEM micrographs of unground sample **CP1**, ground samples (**CP1**-G) and treated samples with CH_3CN (**CP1**-R) for 3 cycles.

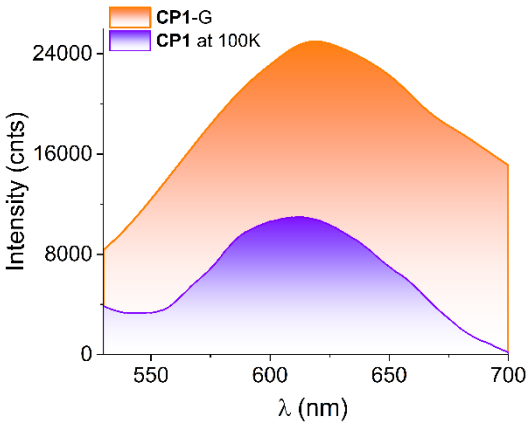

Fig. S15. Emission spectra (λ_{ex}= 425 nm) of **CP1**-G at room temperature and **CP1** at 100 K.

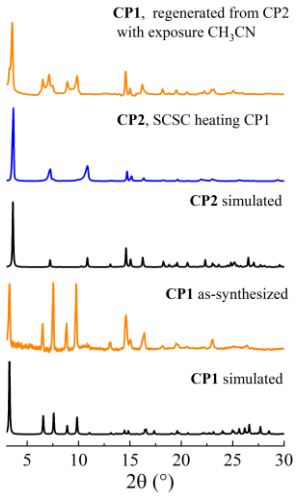

Fig. S16. PXRD (Cu K_α) patterns of the SCSC transformation from **CP1** to **CP2**.

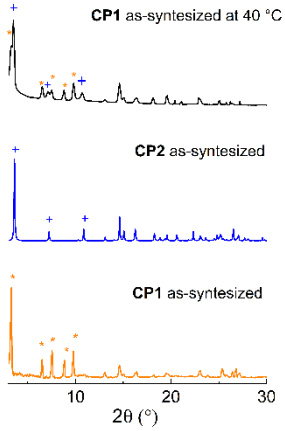

Fig. S17. PXRD (Cu K_α) patterns of **CP1**, **CP2** and **CP1** at ~ 40 °C.

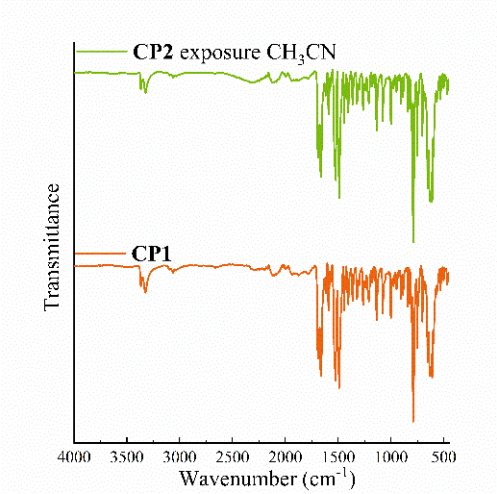

Fig. S18. IR-ATR spectra of crystalline starting sample **CP1** (bottom) and **CP1** (top) regenerated sample from **CP2** exposure in CH_3CN.

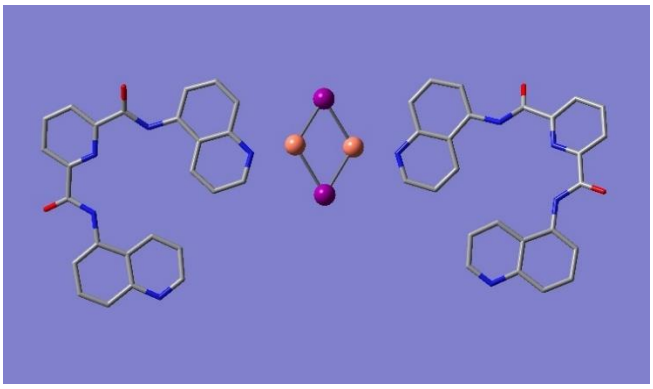

Fig. S19. DFT optimized structure of **CP1** at 100 K.

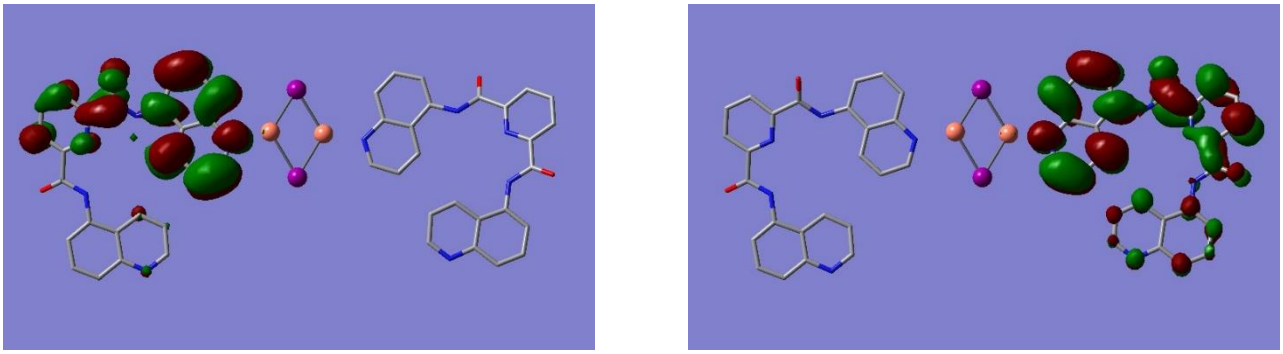

HOMO LUMO

Fig. S20. Molecular orbitals (MOs) for **CP1** using the optimized $[Cu_2(\mu\text{-}I)_2(L)_2]$ fragment.

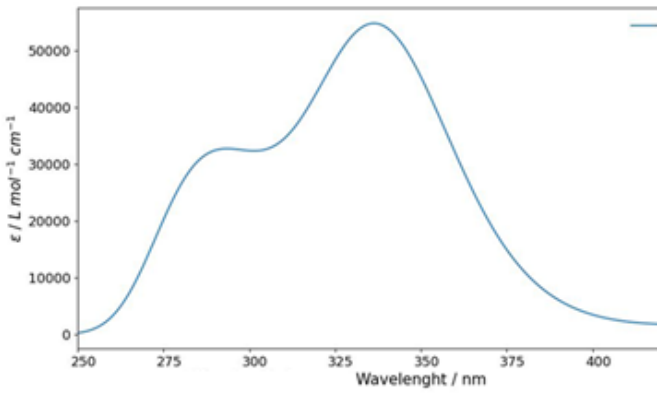

Fig. S21. UV-vis plot of **CP1** calculated with the TD-DFT method at the M052X/LANL2DZ//cc-pVTZ (Iodine) level of theory.

Table S7. Selected excited states calculated at the TD-DFT M05-2X/LANL2DZ //cc-pVTZ (Iodine) level of theory for **CP1** and **CP2**.

Oscillator Strength (*f*)	Transition (% contribution)	Assignment	E (eV)	λ_{calcd} (nm)
CP1 at 100 K				
0.5328	HOMO-5 → LUMO+1 (36) HOMO-7 → LUMO (29)	MLCT IL	4.32	335.11
0.4006	HOMO → LUMO+5 (48) HOMO → LUMO+4 (12)	IL IL	0.98	264.19
0.3000	HOMO-4 → LUMO+2 (13) HOMO-1 → LUMO+2 (67) HOMO-1 → LUMO+5 (19)	MLCT MLCT MLCT	4.34	285.89
0.0851	HOMO → LUMO+9 HOMO → LUMO+10 HOMO → LUMO+7 HOMO → LUMO+12	MLCT CC CC CC	2.47	479.62
CP1 at 293 K				
0.4157	HOMO → LUMO+1	IL	4.37	283.17
0.2843	HOMO-1 → LUMO (44) HOMO-2 → LUMO (41)	IL IL	4.24	292.19
0.4264	HOMO-1 → LUMO+4 (34) HOMO-2 → LUMO+4 (39)	IL IL	5.74	215.80
0.9636	HOMO → LUMO+5 (36) HOMO-1 → LUMO+5 (36)	IL IL	5.86	211.63
CP2				
0.9289	HOMO → LUMO+5 (41) HOMO-5 → LUMO+1 (9) HOMO-5 → LUMO+3 (22)	MLCT IL IL	5.86	211.50
0.4480	HOMO-10 → LUMO (66)	IL	6.78	182.71

Note.- Time Dependent calculations at the aforementioned level of theory was performed requesting 80 states while using the SMD continuum solvation model with acetonitrile as solvent. The SMD solvation model is specifically designed to work with the Minnesota family of functionals as in the present case. Full core pseudopotentials were used for Copper and Iodine while their all-electron version was used for the rest of the atoms in the molecule. Only those transitions with the highest values of oscillator strengths are reported below.

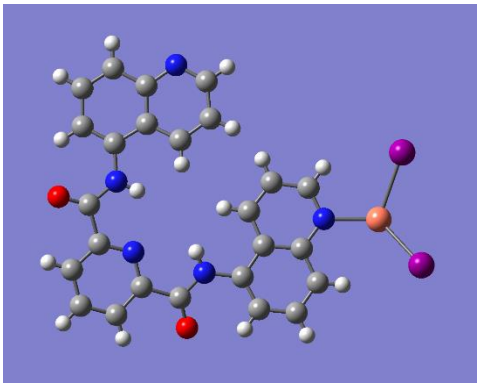

Fig. S22. DFT optimized structure of **CP1** at 293 K.

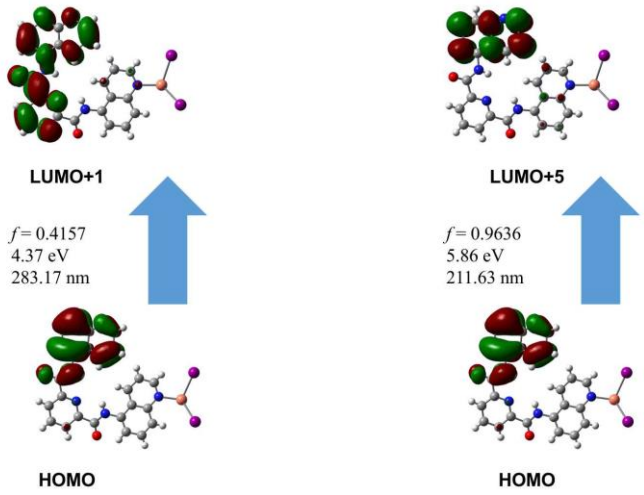

Fig. S23. Representation of selected MOs of the $[Cu_2(\mu\text{-}I)_2(L)_2]$ fragment of **CP1** at 293 K with oscillator strengths (*f*) and energy levels.

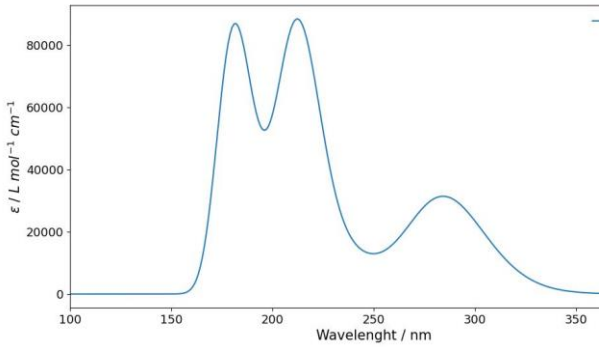

Fig. S24. UV-vis plot of **CP2** calculated with the TD-DFT method at the M052X/LANL2DZ//cc-pVTZ (Iodine) level of theory.

References:

1 J. Valdes-García, J. Zamora-Moreno, M. K. Salomón-Flores, D. Martínez-Otero, J. Barroso-Flores, A. K. Yatsimirsky, I. J. Bazany-Rodríguez and A. Dorazco-González, Fluorescence Sensing of Monosaccharides by Bis-boronic Acids Derived from Quinolinium Dicarboxamides: Structural and Spectroscopic Studies, *J. Org. Chem.*, 2023, **88**, 2174–2189.

2 J. Zamora-Moreno, J. B.-F. María K. Salomón-Flores, Josue Valdes-García, Cristian Pinzón-Vanegas, Diego Martínez-Otero and M. Á. R.-S. and A. D.-G. Raúl Villamil-Ramos, Water-soluble fluorescent chemosensor for sorbitol based on a dicationic diboronic receptor. Crystal structure and spectroscopic studies, *RSC Adv.*, 2023, **13**, 32185–32198.

3 M. J. Frisch, G. W. Trucks, H. B. Schlegel, G. E. Scuseria, M. A. Robb, J. R. Cheeseman, G. Scalmani, V. Barone, G. A. Petersson, H. Nakatsuji, X. Li, M. Caricato, A. V Marenich, J. Bloino, B. G. Janesko, R. Gomperts, B. Mennucci, H. P. Hratchian, J. V Ortiz, A. F. Izmaylov, J. L. Sonnenberg, D. Williams-Young, F. Ding, F. Lipparini, F. Egidi, J. Goings, B. Peng, A. Petrone, T. Henderson, D. Ranasinghe, V. G. Zakrzewski, J. Gao, N. Rega, G. Zheng, W. Liang, M. Hada, M. Ehara, K. Toyota, R. Fukuda, J. Hasegawa, M. Ishida, T. Nakajima, Y. Honda, O. Kitao, H. Nakai, T. Vreven, K. Throssell, J. A. Montgomery Jr., J. E. Peralta, F. Ogliaro, M. J. Bearpark, J. J. Heyd, E. N. Brothers, K. N. Kudin, V. N. Staroverov, T. A. Keith, R. Kobayashi, J. Normand, K. Raghavachari, A. P. Rendell, J. C. Burant, S. S. Iyengar, J. Tomasi, M. Cossi, J. M. Millam, M. Klene, C. Adamo, R. Cammi, J. W. Ochterski, R. L. Martin, K. Morokuma, O. Farkas, J. B. Foresman and D. J. Fox, Gaussian 16 Revision C01, *Gaussian, Inc., Wallingford CT*, 2016, Gaussian, Inc., Wallingford CT:16.

4 Emanuel Contreras-Cuevas, Humberto Estrada-Lara, Joaquín Barroso-Flores, 'UVeh-Vis: a python tool for plotting UV-Vis spectra from excited states calculations' (2023) Git Hub https://github.com/joaquinbarroso/UVeh-Vis.